

# On-line evaluation of measurement results during the determination of residual stress using strain gages

by Stefan Keil

With experimental stress analysis using strain gages the stresses which are required must be computed from the measured strains. These computations may in certain cases be based on complex algorithms, rendering the evaluation particularly complicated and inconvenient. However, the complexity of the evaluation recedes into the background with on-line computer-controlled digital measuring systems and appropriate Software, because all computations and evaluations are executed quickly and reliably by the instrument/computer combination of equipment. The article illustrates an example of an industrial application for residual stress determination based on the ring-core method. The measurement object is a rotor disk for a steam turbine. The author highlights the simplicity of working with an on-line measurement System and HBM's BEAM Software, despite the complicated evaluation algorithm that is involved.

## Introduction

Residual stresses in components have received increasing attention in the last few years. They are mechanical stresses present in the workpiece that are not the result of external forces or moments. Residual stresses can severely impair the load-bearing capacity of a component if they occur with the same arithmetic sign as the load stresses. In contrast, they can contribute to an increase in the load-bearing capability if their arithmetic sign is opposite to that of the load stresses. It follows then, that the most favorable residual stress state in the component is needed to exploit the component's properties to the full.

Residual stresses can arise in a material due to thermal effects (e.g. cooling after casting, rolling, welding or heat treatment), mechanical effects (e.g. cold forming) and due to physical/chemical effects (e.g. grain changes during cooling).

In a body subject to residual stresses there is an internal mechanical equilibrium which can be disturbed by external intervention. This can take the form of drilling a hole such as in the *Hole Drilling Method* or milling an annular groove as in the *Ring-Core Method*. After this disturbance stage a new equilibrium state is established which differs from the previous one. The difference between both states of equilibrium can be measured based on the associated deformation states and it therefore presents a way of determining the residual stresses by applying strain-gage technology.

It is a characteristic of the technique for determining residual stresses with strain gages that only changes in strain can be measured. The stresses causing these changes of strain must then be calculated. The amount of computation required can be considerable, particularly if the residual stress distribution in layers be-

neath the surface of the work-piece is to be found in the form of a depth distribution. The laws governing the linear elastic properties of materials are used as a basis for this type of calculation, together with experimentally determined calibration functions specific to the procedure. The conditional equations for the required residual stress distribution are differential equations which contain the strains measured by three strain gages as functions of the penetration depth of the drill or milling cutter with respect to the depth. In addition, the calibration factors mentioned above must also be considered as depth functions.

Carrying out this type of computation is extremely inconvenient for the practical application of the technique due to the amount of calculation required. With the availability of modern aids such as digital measurement equipment and suitable Software, the amount of calculation work involved is enormously reduced. With measurement systems operating on-line, the distribution of residual stress can now be found very conveniently, because the complete evaluation work is carried out by the Software. Using the ring-core technique as an example, the following shows how easily the determination of residual stresses can be carried out.

## Test object

The test object was a 2.65 t rotor-disk forging for a low-pressure steam turbine which served as the test disk for the optimization of the residual stress state. It also provided a means of testing the on-line evaluation technique in a real application.

Rotors for high performance steam turbines are often designed as a series of disks since the manufacture of very large rotors of sufficient quality from one forging

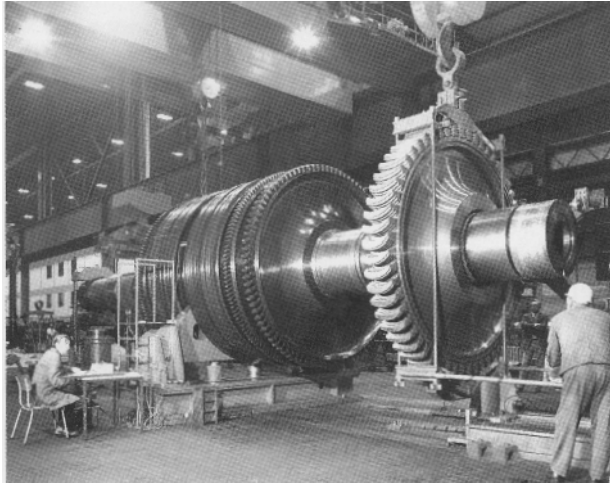


**Fig. 1:** View of a disk-type rotor for a low-pressure steam turbine during assembly.

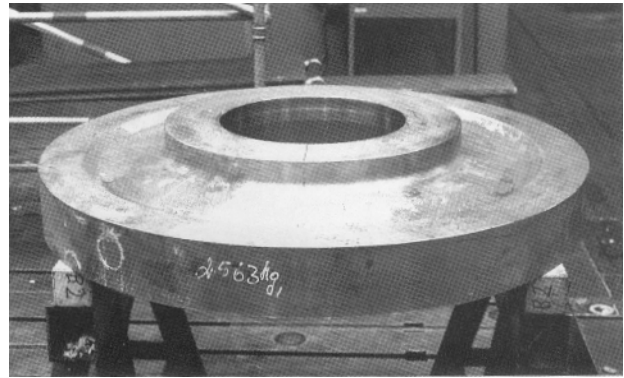


**Fig. 2:** The test object, a 2.56 t forging of a rotor disk for a low-pressure steam turbine.

represents a significant problem. A disk rotor consists of a central spindle onto which separate wheel disks are shrunk. **Figure 1** shows a view of a disk rotor during assembly. The stresses on a turbine disk under operating conditions arise due to shrink-on stresses, tensile stresses due to centrifugal forces, thermal stresses and residual stresses. All these stresses are superimposed on one another in the disk according to their arithmetical sign and should be known for the proper dimensioning of the disk. **Figure 2** shows the disk forging of material 26 NiCrMo V 14 5 supported on trestles ready for the ring-core measurement. Special thanks are due to Siemens AG, Power Engineering Group KWU at Mülheim for their invaluable support during the practical checking of the evaluation software.



**Fig. 3:** View of the RY 51 Ring-Core Rosette showing both sides. An impression of its size can be obtained from the quarter-dollar coin.

Compressive residual stresses in the region of the shrink-on fit are an advantage in the design of the disk, because they oppose the tensile stresses which are unavoidable in shrink fitting. Compressive residual stresses prevent stress-crack corrosion over the complete surface region of the disk. With specific heat treatment of the disk forging during its manufacture, e.g. water spraying in the boring, certain magnitudes and distributions of the residual stresses can be obtained in the disk. The checking of the success of this heat treatment is then carried out using the ring-core method which was developed by Siemens AG, KWU Mülheim. This method is used to find the residual stress distribution at selected measuring points down to a depth of about 5 mm (0.2 in).

During the practical implementation of the technique the support for the device for milling the annular groove is fixed above the center of the previously specified measuring point as shown in **Fig. 4** using a guide plate and a centering pin. The magnetic feet of the support are used for fixing, supplemented by bonding with X60 Two-Component Cement. The guide plate is then removed and the ring-core rosette bonded to the previously prepared measuring point as shown in **Fig. 5** using Z 70 One-Component Cement. Here, care is

## Implementing the technique

A comprehensive description of the ring-core principle will not be given here, since this can be obtained from [1 to 3]. Here, a practical application example is involved with the main feature being the on-line evaluation of the measurement results. The special strain-gage rosette that was used, known as a ring-core rosette, is shown in **Fig. 3** with both top and bottom views. It was patented in 1977 [4].



**Fig. 4:** Central fixing of the support for the milling device above the measuring point.

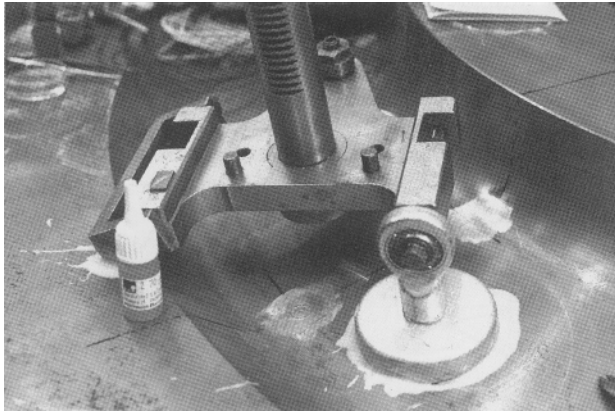


**Fig. 5: Mounting the ring-core rosette at the center of the measuring point.**

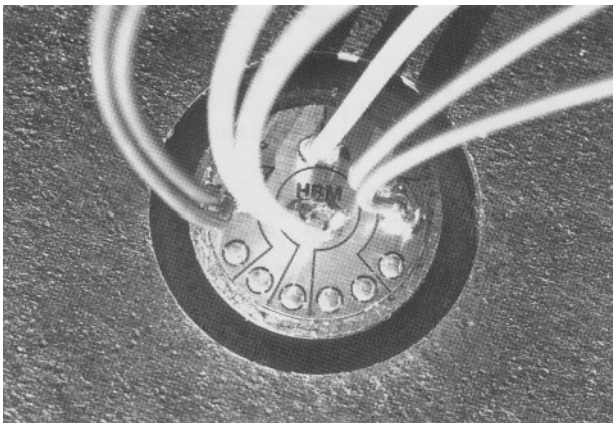


**Fig. 6: Connections to the three rosette measuring grids were implemented in a three-wire configuration.**

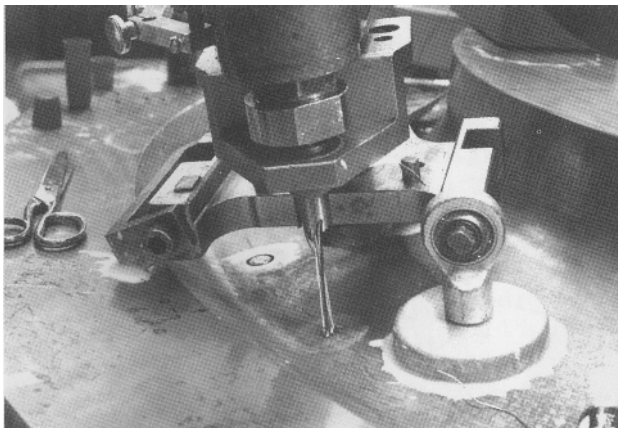


**Fig. 7: Positioning the milling device over the measuring point, passing the leads upwards through the hollow spindle.**

taken to ensure that the three measurement directions of the rosette measuring grids, which are angularly displaced by 45° from one another, are in defined positions with respect to the test object co-ordinates. In the example the rosette reference direction a is aligned radially and the measurement grid c is aligned tangential to the disk shape.

The next step consists of inserting the milling device in the support and passing the leads for the electrical connection of the rosette measuring grids from above through the hollow milling spindle. The cores of the lead are previously stripped and tinned. A three-wire configuration is used with a common return for the three measuring grids. **Figure 6** shows the correct wiring of the rosette in a close-up photograph. When soldering the wires, it should be ensured that they are soldered to the areas of the printed circuit board which acts as a protective cover. The solder points for the internal rosette wiring, which can be seen in the lower part of the rosette in Fig. 6, should not be used for soldering. To protect them from twisting, the leads are lead up through the milling spindle in a protective tube. The milling spindle and connection leads positioned above the ring-core rosette can be seen in **Fig. 7**.

In the next stage the milling spindle is lowered so that the teeth on the cutter contact the surface of the test object prior to the start of milling. All the sensors used for the measurement are zeroed in this position. These are the mechanical dial gage used as a visual operator aid for measuring the cutting depth, the inductive displacement transducer which supplies an electrical signal proportional to the milling depth for the on-line evaluation and the three rosette measuring grids which are wired with a common compensation strain gage to form three half bridges. The zero balancing for these half bridges and for the inductive displacement transducer is carried out automatically at the press of a key by the on-line measurement system used for signal processing and evaluation. **Figure 8** illustrates the milling device mounted at the measuring point together with the dial gage and the displacement transducer. On the right of the milling device is the lever for the manual operation of the cutter feed.

The actual milling process can start after the zero balancing and the cutter is fed manually in steps of about 0.5 mm (0.02 in). Exact conformance to specific depth

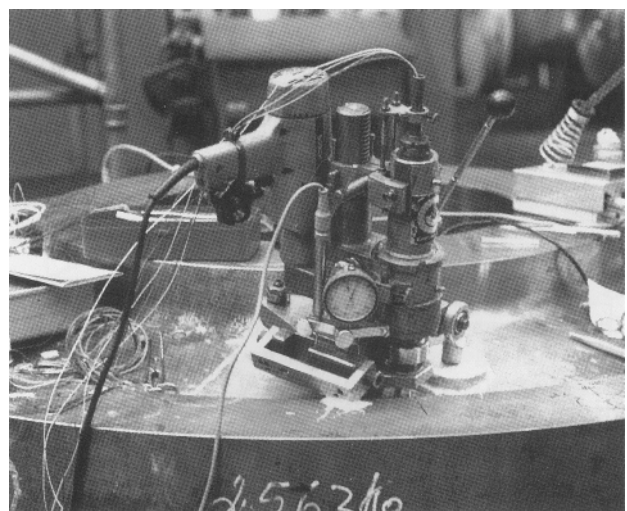


**Fig. 8: View of the milling device on the test object together with the dial gage and inductive displacement transducer for visual and electrical measurement of the milling depth.**

steps is not necessary, since the milling depth is measured at each stage by the inductive displacement transducer and passed to the measurement system for evaluation. During milling it is recommended that the cutting surfaces are lubricated with a little drilling oil applied to the milling point with a brush. The swarf can also be easily removed with the moist brush. After each stage of milling the milling tool is withdrawn from the groove, the swarf removed, the milling tool inserted again to the bottom of the groove and the measurement is triggered by the press of a key on the keyboard of the computer used for the on-line processing of the measurement signals. The removal of swarf by withdrawing the milling tool is necessary, because swarf collects on the printed circuit board on the rosette and may cause short circuits. This can be remedied also by covering the soldering points with a ball of adhesive insulating material, e.g. UHU plus, after soldering the leads to the rosette.

The step-by-step milling was carried out on the disk to an overall depth of 4 mm (0.16 in). After the milling and the transfer of the measurements to the on-line instrument system the ring-core process at this measuring point is finished. The milling equipment is removed and mounted at another measuring point.

## Signal processing

The processing of the measurement signals is carried out with an on-line measurement system consisting of a computer controllable UPM 60 Multi-Point Measuring Unit and an Apple Macintosh computer. A version of BEAM, modified for the ring-core technique, is available for the software. The connection of the strain-gage rosette to the multi-point unit is realized via a terminal to which the completion resistance serving all three measuring points is connected. The inductive displacement transducer is directly connected to the multi-point unit. The terminal and its connection points at the back of the unit are illustrated in Fig. 9. After the milling of each stage the four measuring signals (milling depth and the three strains) are acquired, amplified and conditioned by the multi-point unit and then passed as digital numerical values in their appropriate units to the computer.

## Evaluation

The theory on which the evaluation is based is summarized in [5] together with all the necessary formulas and their derivations. The objective of the evaluation is to display the planar residual stress state at the measuring point under consideration as a function of the depth  $z$ . It is based on equations from the theory of elasticity and on calibration functions specific to the technique which are available to the user if he keeps to the parameters associated with the calibration functions. These parameters are the RY 51 Ring-Core Rosette, the shape of the milling tool and Poisson's ratio for the test object material.

The complete evaluation can be reduced to a few equations. The strains  $\varepsilon_a$ ,  $\varepsilon_b$  and  $\varepsilon_c$  are measured in the three measurement directions designated a, b and c as a function of the milling depth  $z$ . The three residual stresses to be determined in these directions have the following relationship to the depth  $z$ :

$$\sigma_a(z) = \frac{E}{K_1^2(z) - \nu^2 K_2^2(z)} \left[ K_1(z) \frac{\Delta \varepsilon_b(z)}{\Delta z} + \nu K_2(z) \frac{\Delta \varepsilon_c(z)}{\Delta z} \right] \quad (1)$$

$$\sigma_b(z) = \frac{E}{K_1^2(z) - \nu^2 K_2^2(z)} \left[ K_1(z) \frac{\Delta \varepsilon_b(z)}{\Delta z} + \nu K_2(z) \left( \frac{\Delta \varepsilon_a(z)}{\Delta z} - \frac{\Delta \varepsilon_b(z)}{\Delta z} + \frac{\Delta \varepsilon_c(z)}{\Delta z} \right) \right] \quad (2)$$

$$\sigma_c(z) = \frac{E}{K_1^2(z) - \nu^2 K_2^2(z)} \left[ K_1(z) \frac{\Delta \varepsilon_c(z)}{\Delta z} + \nu K_2(z) \frac{\Delta \varepsilon_a(z)}{\Delta z} \right] \quad (3)$$

The calibration functions  $K_1(z)$  and  $K_2(z)$  with the differential coefficients  $\Delta \varepsilon_i(z)/\Delta z$  must be substituted in these equations. This is carried out automatically for each depth stage by the computer program. The values for the differential coefficients are produced after the milling of each depth stage from the measurements at the start and end of the stage milling.

The calibration functions  $K_1(z)$  and  $K_2(z)$  are available initially as experimentally determined tables of values [6]. In order to be able to incorporate these in the software as continuous functions, the tables of values were substituted by approximation polynomials.

$$K_i = a_0 + a_1 z + a_2 z^2 + a_3 z^3 + a_4 z^4 + a_5 z^5 + a_6 z^6 + \dots \quad (4)$$

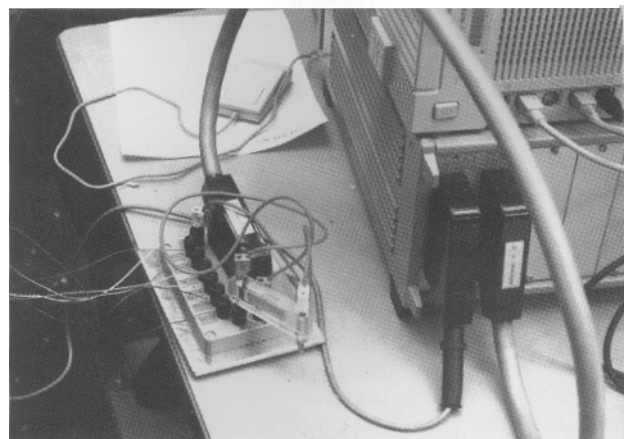


Fig. 9: Connection of the measuring leads to the UPM 60 Multi-Point Measuring Unit via a terminal with a common completion resistor for half bridge circuits.

Figure 10 shows the curves for the two calibration functions. The values for the coefficients for  $K_1(z)$  and  $K_2(z)$  are summarized in Table 1. Both calibration functions  $K_1$  and  $K_2$  can be taken from the algebraically formulated calibration functions for any depth  $z$ . This also takes place automatically in the computer program.

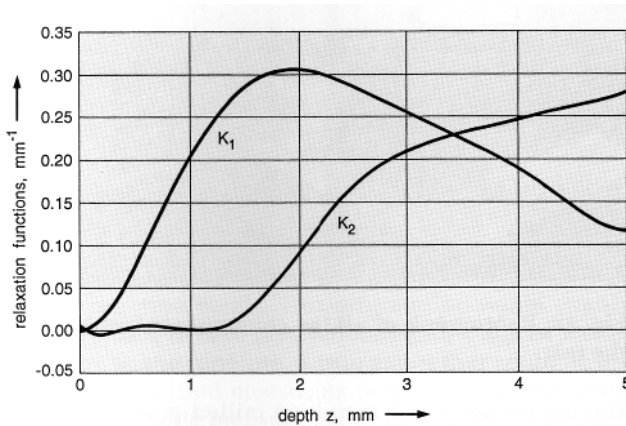


Fig. 10: Calibration functions as graphical representations of approximation polynomials.

	Coefficients for $K_1$	Coefficients for $K_2$
$\alpha_0$	0.000490	0.003857
$\alpha_1$	-0.041198	-0.139130
$\alpha_2$	0.577240	0.740230
$\alpha_3$	-0.466690	-1.451100
$\alpha_4$	0.155810	1.351200
$\alpha_5$	-0.024250	-0.681520
$\alpha_6$	0.001448	0.194900
$\alpha_7$		-0.032032
$\alpha_8$		0.002818
$\alpha_9$		-0.000103

Table 1: Coefficients in the approximation polynomial for the calibration functions  $K_1(z)$  and  $K_2(z)$ .

After the three stress components  $\sigma_a$ ,  $\sigma_b$  and  $\sigma_c$  have been found, the calculation of the principal stresses  $\sigma_1$  and  $\sigma_2$  for the planar residual stress state and the angle of orientation  $\varphi$  for the principal direction 1 is trivial. It is found by the program according to the equations

$$\sigma_{1,2}(z) = \frac{\sigma_a(z) + \sigma_c(z)}{2} \pm \frac{1}{2} \sqrt{2 \sqrt{[\sigma_b(z) - \sigma_a(z)]^2 + [\sigma_b(z) - \sigma_c(z)]^2}} \quad (5)$$

$$\varphi = \frac{1}{2} \arctan \frac{2\sigma_b(z) - \sigma_a(z) - \sigma_c(z)}{\sigma_a(z) - \sigma_c(z)} \quad (6)$$

With the BEAM graphical user environment the program is very easy to use. The operator guidance is easy

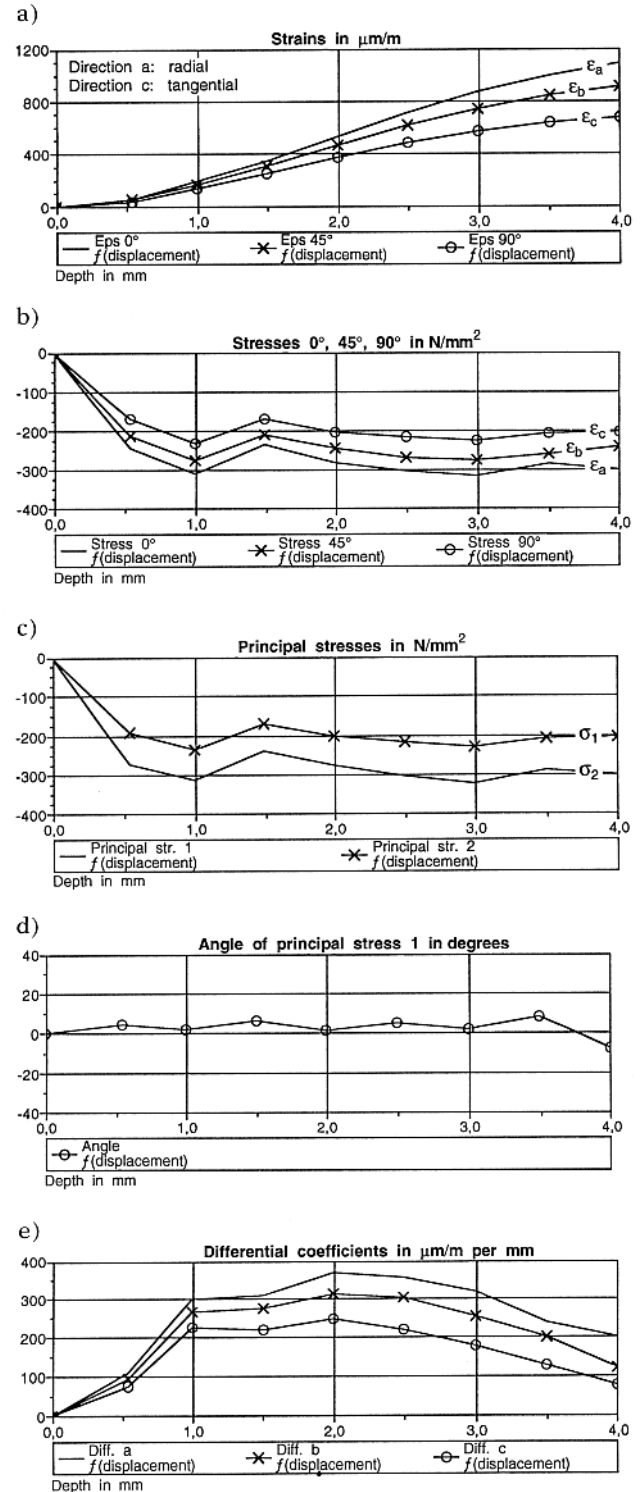


Fig. 11: Examples of the graphical display of the results; taking the diagrams from top to bottom:

- a) measured strains
- b) computed stress components
- c) principal stresses of the residual stress state
- d) orientation angle of principal direction 1
- e) differential coefficients of the strains for the depth stages

to understand and the user does not need any programming knowledge. Even someone untrained in using computers can easily operate the program after a very brief introduction. The many graphical and tabular displays provided by the program enable the selection of various presentations for the results and direct online logging.

Stress analysis using the ring-core method  
11th July 1990, Siemens KWU, Mülheim

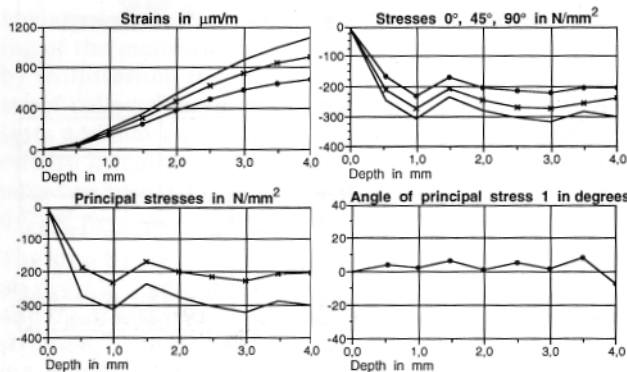


Fig. 12: Black and white hard-copy of the coloured screen contents at the end of the residual stress determination.

The display of the results for the residual stress determination described here is produced graphically during the test. New results were included in the display after the completion of each depth stage. The measured strains  $\epsilon_a$ ,  $\epsilon_b$  and  $\epsilon_c$ , together with the corresponding stresses  $\sigma_a$ ,  $\sigma_b$  and  $\sigma_c$  computed using equations (1) to (3), the principal stresses  $\sigma_1$  and  $\sigma_2$  of the planar residual stress state and the orientation angle  $\varphi$  to the principal direction 1 were all displayed in graphs with the abscissa representing the milling depth  $z$ .

The principal direction 1 is rotated by the angle  $\varphi$  in the mathematical positive sense with respect to the rosette reference direction  $a$ . In addition, the individual differential coefficients  $\Delta\epsilon_i / \Delta z$  can also be displayed. The values found on the rotor disk forging, output as a graphical log, are shown under a) to e) in Fig. 11. A hard-copy of the screen contents as obtained on the monitor at the end of the measurement is reproduced in Fig. 12. Figure 13 shows a photograph of all components involved in the practical implementation of the technique.

## Conclusion

The example given here shows how easy the evaluation of a ring-core test can be using modern on-line measurement technology. The procedure explained for one measuring point can now be applied to other measuring points to obtain information about the residual stress distribution, for example, along the contour of a radial section of the disk.



Fig. 13: Photograph of all the components involved in the test.

The approximately 4 mm deep milled grooves in the surface of the disk forging were cut away during the following mechanical machining operation, so that no traces of the application of the technique remained. Therefore, the ring-core technique can be regarded in this case as a quasi non-destructive method.

## References

- [1] Wolf, H., Böhm, W.: Das Ringkern-Verfahren zur Messung von Eigenspannungen und seine Anwendungen bei Turbinen- und Generatorwellen; Arch. f. d. Eisenhüttenw. 42 (1971), pp. 195-200
- [2] Wolf, H., Böhm, W.: Entstehung, Messung und Beurteilung von Eigenspannungen in schweren Schmiedestücken für Turbinen und Generatoren; Arch. f. d. Eisenhüttenw. 42 (1971), pp. 509-513
- [3] Böhm, W., Stücker, E., Wolf, H.: Grundlagen und Anwendungsmöglichkeiten des Ringkern-Verfahrens zum Ermitteln von Eigenspannungen, Teil 1: Theorie und Grundlagen; MTB 16 (1980), pp. 36-40
- [4] Böhm, W., Stücker, E., Wolf, H.: Dehnungsmeßstreifen zur Messung von Oberflächendehnungen an kreisflächenförmigen Werkstückabschnitten; Patent doc. 23 45 309, issued 17.11.1977
- [5] Keil, S.: Experimental determination of residual stresses with the ring-core method and an on-line measuring system; Experimental Techniques Sept./ Oct. 1992, pp. 17-24
- [6] Stücker, E.: Personal memo 1990.

Dr.-Ing. Stefan Keil is a senior engineer at Hottinger Baldwin Messtechnik GmbH, Darmstadt, FRG with special responsibility for experimental mechanics. He is also the editor of RAM.